JACS
JOURNAL OF THE AMERICAN CHEMICAL SOCIETY
pubs.acs.org/JACS
Article

A Spectroscopically Observed Iron Nitrosyl Intermediate in the Reduction of Nitrate by a Surface-Conjugated Electrocatalyst

Moumita Ghosh, Sarah E. Braley, Roman Ezhov, Harrison Worster, Juan A. Valdez-Moreira, Yaroslav Losovyj, Elena Jakubikova,* Yulia N. Pushkar,* and Jeremy M. Smith*

Cite This: J. Am. Chem. Soc. 2022, 144, 17824−17831
Read Online

ACCESS | Metrics & More | Article Recommendations | Supporting Information

ABSTRACT: We report an iron-based graphite-conjugated electrocatalyst (GCC-FeDIM) that combines the well-defined nature of homogeneous molecular electrocatalysts with the robustness of a heterogeneous electrode. A suite of spectroscopic methods, supported by the results of DFT calculations, reveals that the electrode surface is functionalized by high spin (S = 5/2) Fe(III) ions in an FeN_4Cl_2 coordination environment. The chloride ions are hydrolyzed in aqueous solution, with the resulting cyclic voltammogram revealing a Gaussian-shaped wave assigned to $1H^+/1e^-$ reduction of surface Fe(III)−OH surface. A catalytic wave is observed in the presence of NO_3^-, with an onset potential of −1.1 V vs SCE. At pH 6.0, GCC-FeDIM rapidly reduces NO_3^- to ammonium and nitrite with 88 and 6% Faradaic efficiency, respectively. Mechanistic studies, including *in situ* X-ray absorption spectroscopy, suggest that electrocatalytic NO_3^- reduction involves an iron nitrosyl intermediate. The Fe−N bond length (1.65 Å) is similar to that observed in {Fe(NO)}^{6} complexes, which is supported by the results of DFT calculations.

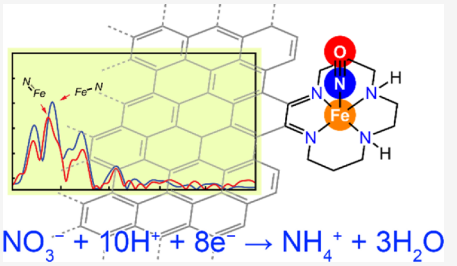

INTRODUCTION

Since the introduction of the industrial Haber−Bosch process in 1913, humans have doubled the annual rate of nitrogen entering the planet's nitrogen cycle, with anthropological sources now dominating the production of bioavailable nitrogen.[1,2] While this nitrogen is critical for feeding the planet, primarily in the form of NH_3-based fertilizer, these massive influxes have led to deleterious environmental consequences.[3,4] It is estimated that only 17% of the 135 million tons of annual agricultural nitrogen is retained as vegetable and meat protein.[2] Most significantly, soil organisms convert almost half of the applied NH_3 fertilizer to highly soluble nitrate, whose runoff into waterways leads to large-scale pollution of ecosystems (the "Nitrogen Cascade"), altering their function and the living communities they support.[5−7] Nitrate runoff also contaminates aquifers and, consequently, drinking water—with potentially serious threats to human health.[8]

Since biological denitrification processes are overwhelmed by anthropogenic nitrate, there is an opportunity to develop new methods for recycling nitrate by converting it to useful or benign compounds. Indeed, the 2017 United Nations World Wastewater Report has recognized agricultural wastewater as an untapped resource for useful organic chemicals.[9] Due to the enormous energy demands of global NH_3 production, efficient methods of nitrogen recycling are likely to have significant energy consequences.

Electrocatalytic methods for nitrate reduction represent one strategy for addressing these issues. Nitrate reduction is a multielectron, multiproton process. Although thermodynamically favorable, there are unique challenges associated with the reduction of nitrate in aqueous solution. Nitrate is a weakly binding and kinetically inert species that has complex redox chemistry because (1) the low charge density and delocalized electronic structure significantly attenuate its nucleophilicity and electrophilicity, making it a poor catalyst substrate, particularly in comparison with other ions commonly found in aqueous solutions;[10] (2) its negative charge introduces a kinetic barrier to reduction; and (3) the relative stability of many nitrogen oxidation states means that multiple reduction products are possible, some of which have very similar reduction potentials.[11] Consequently, there are few examples of selective and efficient electrocatalysts for the reduction of aqueous nitrate.[12−16]

Aqueous nitrate can be electrochemically reduced on heterogeneous metal or alloy electrodes, typically with large overpotentials and with low product selectivity.[17,18] Here, the catalytic activity and selectivity are often strongly dependent on the electrolyte composition and pH, with little opportunity for tuning catalyst performance. While recent work has highlighted potential advantages for certain alloys,[19] composite

Received: March 31, 2022
Published: September 26, 2022

https://doi.org/10.1021/jacs.2c03487
J. Am. Chem. Soc. 2022, 144, 17824−17831

Scheme 1. Synthesis of GCC-FeDIM

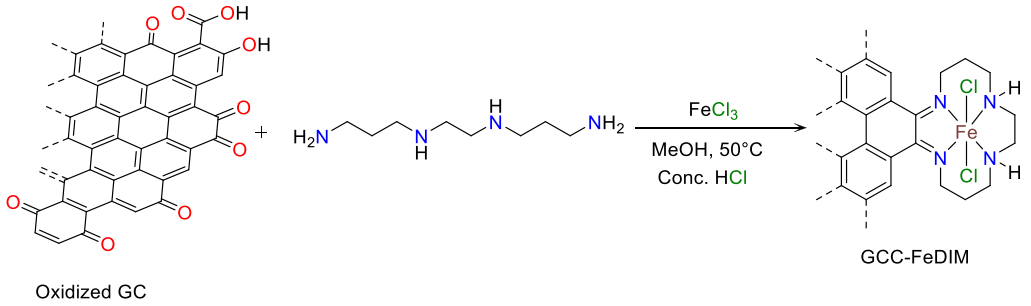

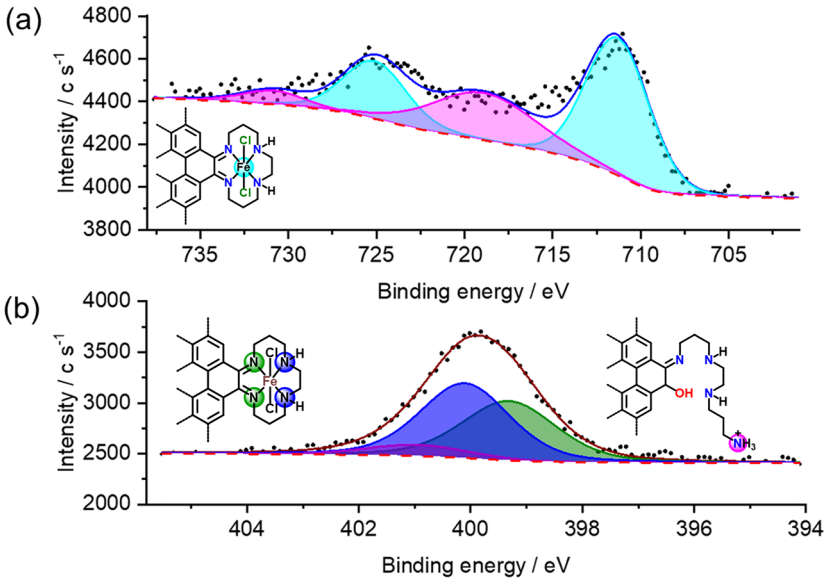

Figure 1. (a) High-resolution Fe 2p XPS spectrum of GCC-FeDIM (glassy carbon). The measured signal is in black, the overall fit manifold is in blue, and the fit peaks are in magenta and cyan; (b) High-resolution N 1s XPS spectrum of freshly prepared GCC-FeDIM. The measured signal is in black, the fit peaks are in green, blue, and purple, and the overall fit manifold is in blue. The proposed structures of GCC-FeDIM and protonated amine sites on the surface are also shown.

materials,[20,21] nanomaterials,[19] and "single-atom" catalysts,[22] the structural diversity of these catalysts, coupled with the lack of mechanistic insight, makes the rational improvement of performance difficult.

By contrast, the tunability of molecular electrocatalysts makes them well-suited for developing structure/function relationships that allow for tailored catalyst performance. For example, systematic studies into electrocatalytic nitrate reduction by cobalt-containing macrocycles have provided insight into important catalyst design features.[10,12,23] These complexes reduce aqueous nitrate to hydroxylamine and/or ammonia, with the catalytic performance dictated by macrocycle redox non-innocence, flexibility, and the presence of proton shuttles.

Homogeneous electrocatalysts require sequential electron transfer and substrate activation steps for substrate reduction.[24,25] Therefore, the driving force for substrate conversion is determined by the redox properties of the catalyst. For example, the large overpotential required for nitrate reduction by $[Co(cyclam)Cl_2]^+$ stems from the highly cathodic potential that is required to access the Co(I) state.[12] On the other hand, heterogeneous electrocatalysts have strong electronic coupling throughout the electrode band structure, allowing for concerted electron transfer and substrate activation, which in turn allows for high substrate turnover.[25]

In principle, heterogenization of molecular electrocatalysts allows for the creation of materials that feature tunable molecular sites that are strongly coupled to the electrode band structure. A number of strategies for attaching molecular sites to electrodes have been reported, including noncovalent immobilization of the catalyst on an electrode surface, grafted functionalized aryl radicals on a carbon surface, and covalent attachment of molecules to electrodes through an ethynyl linkage.[26−29] However, the weak physisorption/electrostatic interaction or strong covalent interactions associated with these strategies lead to poor coupling between electrode and attached fragment.[25,30]

Recently, the Surendranath group introduced a new strategy for immobilizing catalysts on an electrode surface. The native surface features of an oxidized glassy carbon electrode are used to construct pyrazine units that are integrated into the conjugated graphite surface.[31] This strategy can be manipulated to conjugate transition-metal-based macrocyclic electrocatalysts. We recently adapted this strategy to the creation of a graphite-conjugated catalyst, GCC-CoDIM, in which the macrocycle is integrated into the graphite electrode.[32] The heterogeneous graphite-conjugated cobalt catalyst reduces aqueous nitrite to ammonium at >99% Faradaic efficiency and with a fast rate (TOF = 19.9 s^{-1}).[32] Despite this excellent

https://doi.org/10.1021/jacs.2c03487
J. Am. Chem. Soc. 2022, 144, 17824−17831

catalytic performance, GCC-CoDIM is not active for the electrocatalytic reduction of aqueous nitrate.

In contrast to the synthesis of many macrocycle complexes, GCC-CoDIM is assembled in two discrete steps, i.e., the macrocycle is assembled at the electrode prior to metalation by cobalt. The discrete cyclization and metalation steps provide a pathway for other metals to be similarly conjugated to the electrode. In this work, we report on the synthesis and characterization of the iron-containing congener, GCC-FeDIM. This electrode is highly active for the reduction of aqueous nitrate, producing ammonium as the major product with high Faradaic efficiency (88%). Mechanistic investigations, including electrochemical, *in situ* X-ray absorption, and computational methods, provide evidence that an iron nitrosyl is formed as a key intermediate in the electrocatalytic reduction of nitrate by GCC-FeDIM.

RESULTS AND DISCUSSION

Synthesis and Characterization of GCC-FeDIM. The graphite-conjugated macrocycle catalyst GCC-FeDIM was synthesized similarly to the previously reported GCC-Co(DIM) catalyst.[32] Specifically, anodically-treated carbon electrodes are treated with 1,2-bis(3-aminopropylamino)-ethane under acidic conditions, followed by metalation with methanolic Fe(III) (Scheme 1). Nonmacrocyclic imine and/or physisorbed species are removed by a washing procedure, which is followed by a cathodic cleaning step to remove adsorbed chloride.

X-ray photoelectron spectroscopy (XPS) of GCC-FeDIM on a glassy carbon electrode shows the presence of Fe and N in an approximately 1:4 ratio. These elements are not observed in the XPS of unmodified or oxidized electrodes (Figures S35 and S36). High-resolution XPS spectra exhibit peaks corresponding to Fe 2p and N 1s. The Fe 2p spectrum displays $2p_{3/2}$ and $2p_{1/2}$ peaks at 711.3 and 725.1 eV, respectively, and their corresponding satellites at 718.9 and 730.9 eV (Figure 1a). These binding energies are consistent with Fe(III).[33] The N 1s spectrum shows three peaks at 399.3, 400.1, and 400.9 eV, corresponding to imine, amine, and protonated amine, respectively (Figure 1b).[32,34] The low chloride content observed by XPS suggests that the chloride ligands are labile, similar to our observations for GCC-CoDIM.[32] In support of this hypothesis, the XPS of a GCC-FeDIM electrode that was not subjected to the cathodic cleaning step but was instead soaked in 1 M NaOTf solution similarly reveals low chloride content. The results of DFT calculations performed for a model system also support this ligand lability. With the carbon electrode truncated to a phenylenediimine moiety (Figure S48), chloride ligand substitution at iron is calculated to be thermodynamically favorable (Figure S49).

Fe K-edge X-ray absorption spectroscopy (XAS) was used to study the oxidation state and coordination environment of the Fe center in FeDIM-modified Grafoil (flexible graphite). The pre-edge feature at 7713.4 eV and edge position at 7132.9 eV in the Fe K-edge X-ray absorption near edge spectrum (XANES) correspond to an Fe(III) center in an octahedral environment (Figure 2).[35]

A fit to the extended X-ray absorption fine structure (EXAFS) spectrum of GCC-FeDIM shows excellent agreement with the proposed chemical environment of the iron center in the conjugated electrode (Table S1 and Figure S31). Here, EXAFS fits indicate four N and two Cl atoms in the first shell, which is a perfect match with the proposed coordination

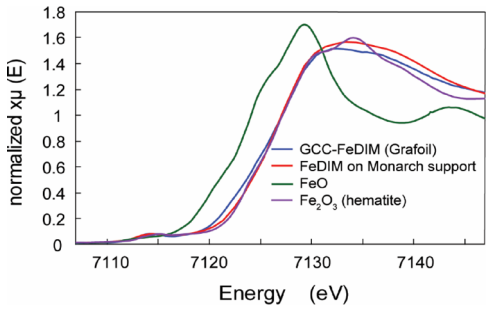

Figure 2. Fe K-edge XANES of freshly prepared FeDIM-modified Grafoil (flexible graphite) electrode and Fe-DIM modified Monarch carbon powder compared with FeO and Fe_2O_3 (hematite) reference compounds.

environment of the iron center (Table S1 and Figure S31a,b). The bond distances between Fe−N and Fe−Cl are 2.10 and 2.22 Å, respectively. Although the analogous molecular complex $[Fe(DIM)Cl_2]^+$ is not known, these distances are in good agreement with those observed for high-spin iron(III) polyazamacrocycle complexes.[36−38] Together, the XPS and XAS data are consistent with the conjugation of molecular $[Fe(DIM)Cl_2]^+$ to the graphite electrode surface. Similarly, GCC-FeDIM conjugation to high-surface area Monarch carbon black powder is supported by Fe K-edge XAS spectra (Figure 2, Table S2, and Figure S31c,d).

Additional spectroscopic methods support the XPS and XAS structural assignments. A signal at $g \approx 4.32$ in the solid-state X-band EPR spectrum of GCC-FeDIM (10 K, Monarch powder) is consistent with high spin ($S = 5/2$) Fe(III) (Figure S29). At 80 K, the zero field ^{57}Fe Mössbauer spectrum of ^{57}Fe-enriched GCC-FeDIM on Monarch carbon black powder can be fit by two quadrupole doublets, with no evidence for metallic iron (Figure S43). The spectral parameters for the major ($\delta = 0.52$ mm s^{-1}, $\Delta E_Q = 0.76$ mm s^{-1}) and minor subspectra ($\delta = 0.61$ mm s^{-1}, $\Delta E_Q = 1.76$ mm s^{-1}) are consistent with high spin ($S = 5/2$) Fe(III).[39,40] The relative areas of the two subspectra are the same at 80 and 200 K, which rules out a temperature-dependent spin state change. Since chloride ligand exchange is observed (see above), we have tentatively assigned the two subspectra to be from $[FeDIM)Cl_2]$ and $[FeDIM)Cl(OH)]$ sites that are conjugated to the electrode surface. These assignments are supported by DFT calculations for a model complex (Figure S48 and Table S6).

Electrochemical Properties of GCC-FeDIM. The cyclic voltammogram (CV) of GCC-FeDIM in aqueous solution reveals a broad Gaussian-shaped wave ($E_{1/2} = -0.22$ V *vs.* SCE) (Figure 3a), whose peak current shows a linear dependence on the scan rate, indicative of a surface-based redox process (Figure S2). The process is reversible, with a small peak-to-peak separation (62 mV) that further supports the redox behavior being surface-based. Importantly, the CVs of independently prepared GCC-FeDIM electrodes are identical (Figure S5) and differ from that for an oxidized glassy carbon electrode (Figure S6). Integration of this redox wave allows the surface coverage of GCC-FeDIM to be determined (Figure S3). Considering the wave as resulting from a single electron transfer process provides a surface coverage of 0.51 nmol cm^{-2}, which is comparable to that for the recently reported GCC-CoDIM electrode.[32] It is notable that the potential of this wave is pH-dependent, with increasing pH leading to a cathodic shift of the potential.

https://doi.org/10.1021/jacs.2c03487
J. Am. Chem. Soc. 2022, 144, 17824−17831

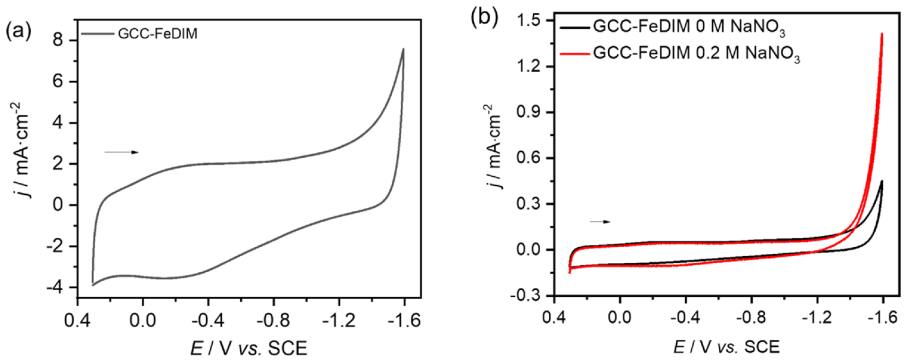

Figure 3. (a) Cyclic voltammogram of GCC-FeDIM (glassy carbon) in 0.5 M Na_2SO_4, pH 6.0, scan rate 100 mV/s; (b) cyclic voltammograms of GCC-FeDIM (glassy carbon) recorded in 0.5 M Na_2SO_4 solution (black), with 0.2 M $NaNO_3$ (red), scan rate 5 mV/s, pH 6.0.

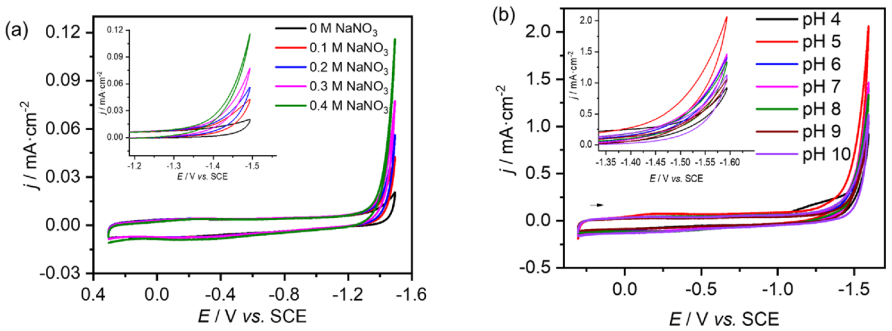

Figure 4. (a) Cyclic voltammograms of GCC-FeDIM (glassy carbon) recorded in 0.5 M Na_2SO_4 with different $NaNO_3$ concentrations, scan rate = 5 mV/s; (b) cyclic voltammograms of GCC-FeDIM (glassy carbon) recorded in 0.5 M Na_2SO_4 at different pH with 0.2 M $NaNO_3$, scan rate = 5 mV/s.

The resulting plot of $E_{1/2}$ *vs.* pH is linear with a slope of 53 mV/dec (Figure S21), suggesting a proton-coupled electron transfer to afford an aqua ligand.[41] This hypothesis is supported by the results of DFT calculations for the model system (Figure S50 and Table S10). At pH 6, only one pathway with a potential similar to that observed experimentally can be identified, where proton transfer is coupled to reduction of the supporting ligand, L:

$$[Fe^{III}(L)Cl(OH)]^+ + H^+ + e^- \rightarrow [Fe^{III}(L^-)Cl(H_2O)]^+$$

$$E = -0.17 \text{ V vs. SCE}$$

In contrast to GCC-CoDIM, GCC-FeDIM is highly active toward the reduction of aqueous nitrate. With 0.5 M Na_2SO_4 electrolyte, the cyclic voltammogram of GCC-FeDIM exhibits a large catalytic current in the presence of 0.2 M $NaNO_3$, (with onset) *ca.* −1.16 V *vs.* SCE (Figure 3b, red; see also Figure S7). No catalytic current is observed in the absence of $NaNO_3$ (Figure 3b, black).

As expected for an electrocatalytic process, increasing the nitrate concentration results in increased catalytic current (Figure 4a). This also indicates that the current enhancement is due to nitrate reduction, not the competitive hydrogen evolution reaction. It is notable that the current enhancement is only observed at slow scan rates (≤100 mV/s), similar to electrocatalytic nitrate reduction by a related molecular electrocatalyst.[12] Nitrate reduction is observed over a wide pH range, with GCC-FeDIM showing highest catalytic activity at pH = 5. The catalyst is poorly active below pH = 3 and above pH = 12 (Figure 4b).

The electroreduction products were determined following 2 h of controlled potential electrolysis (CPE) at −1.31 V *vs.* SCE (Figure S22). Ammonia was determined to be the major electroreduction product with 88% Faradaic efficiency *via* the indophenol test,[42] with no evidence for the formation of NH_2OH. Nitrite was determined to be a minor electroreduction product and formed with 6% Faradaic efficiency as determined by ion chromatography. A similar CPE of NO_2^- at −1.31 V *vs.* SCE for 2 h provided ammonia with quantitative (>99%) Faradaic efficiency, suggesting that free nitrite is formed as an intermediate in the electrocatalytic reduction of nitrate by GCC-FeDIM (Figure S23). It is also notable that GCC-FeDIM selectively reduces nitrate with almost no hydrogen evolution (the Faradaic efficiency for H_2 is 0.17%; Figure S27).

These results allowed the turnover frequency for ammonia formation by GCC-FeDIM to be determined, TOF = 5.2 s^{-1}. Thus, GCC-FeDIM is one to two orders of magnitude faster than two recently reported iron-based single atom catalysts, which operate under similar conditions (TOF = 0.46 and 0.0138 s^{-1}).[22,43]

Several control experiments were conducted to rule out the formation of adsorbed or electrodeposited iron that is leached from GCC-FeDIM. Zero-valent iron is known to reduce aqueous nitrate.[44] Here, it is worth noting that the glassy carbon electrode will reduce nitrate to nitrite, as we have previously reported (Figure S8);[45] however, the onset potential for the bare electrode is 100 mV more anodic than for GCC-FeDIM. This electroreduction activity can be restored by polishing the GCC-FeDIM electrode (Figures S11 and S15).

While we do observe a catalytic current when iron is electrodeposited at the oxidized electrode in the presence of nitrate,[46] the onset potential for catalysis is shifted anodically

https://doi.org/10.1021/jacs.2c03487
J. Am. Chem. Soc. 2022, 144, 17824−17831

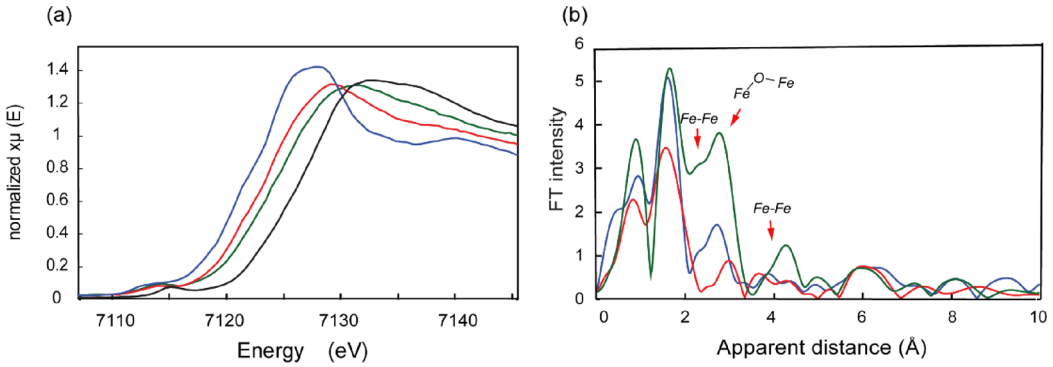

Figure 5. *In situ* Fe K-edge (a) XANES of initial GCC-FeDIM modified Grafoil electrode initial (black) and the same electrode measured at −0.61 V (green), −1.01 V (red), and −1.31 V (blue) *vs.* SCE in 0.5 M Na_2SO_4 electrolyte; (b) EXAFS of GCC-FeDIM Grafoil electrodes at −0.61 V (blue), −1.01 V (red) and −1.31 V (green) *vs.* SCE applied potentials in 0.5 M Na_2SO_4 electrolyte. Significant EXAFS modification only occurs at −1.31 V *vs.* SCE and indicates new Fe−Fe and Fe−O−Fe interactions.

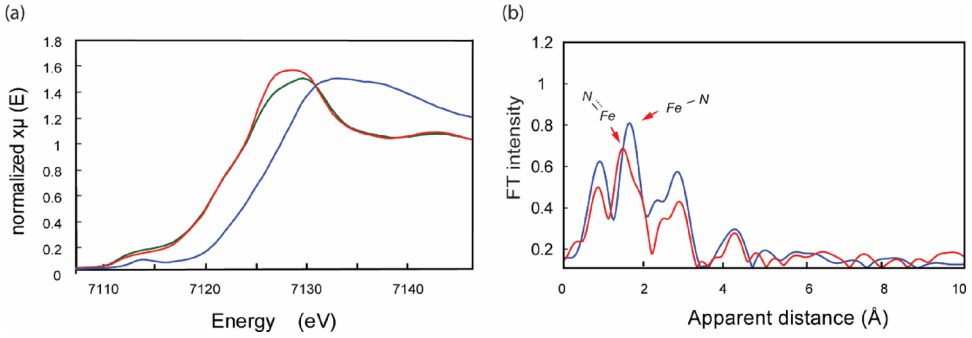

Figure 6. Comparison of XANES (a) and EXAFS (b) for GCC-FeDIM Grafoil with (green) and without 20 mM $NaNO_3$ (red) after 3 h of CPE at −1.31 V *vs.* SCE. Blue in (a) is GCC-FeDIM initial before catalysis.

by 200 mV from that observed for GCC-FeDIM (Figure S9). Moreover, the waveform under these conditions differs considerably from that for GCC-FeDIM. Together, this suggests that metallic iron is not formed in the CV experiments involving GCC-FeDIM. This conclusion is also supported by the results of XAS and XPS experiments, which do not reveal the formation of metallic iron (see below).

Moreover, CPE experiments reveal that electrodeposited iron is a poor catalyst for nitrate reduction. Electrocatalysis at −1.31 V *vs.* SCE (the same potential that was used for GCC-FeDIM) for 2 h provides ammonium with only 39% Faradaic efficiency (Figure S14). Moreover, considerable gas evolution is observed under these conditions. Importantly, the CV for GCC-FeDIM after 2 h of CPE reveals that there is no shift in the onset potential for electrocatalysis (Figure S24). Together, these results are most consistent with GCC-FeDIM being the catalyst for electrochemical nitrate reduction.

Mechanistic Investigations. A number of iron-based heterogeneous electrocatalysts for nitrate reduction are known; however, mechanistic insight is limited to the results of computational investigations, where iron nitrosyl intermediates are proposed as reaction intermediates.[22,43,47,48] The reactivity of homogeneous complexes can provide insight into the reaction mechanisms of heterogeneous catalysts. While a small number of iron complexes have been reported to stoichiometrically reduce nitrate, it is notable that a variety of iron-containing products are observed, including oxo,[49,50] nitrosyl,[51] and dinitrosyl[52,53] complexes. Since these observations suggest that multiple reaction pathways are possible, we undertook a series of electrochemical *in situ* spectroscopic and DFT investigations to probe for reaction intermediates in the electrocatalytic reduction of nitrate by GCC-FeDIM.

In Situ XAS Investigation. Iron K-edge *in situ* XAS was used to observe chemical transformations of the catalyst immobilized on GCC-FeDIM Grafoil electrodes during the electrocatalytic reduction with and without NO_3^- substrate (Figures 5 and 6). *In situ* XANES measurements at different applied potentials (i.e., −0.61, −1.01, and −1.31 V *vs.* SCE reference electrode) indicated a gradual Fe K-edge shift to that of Fe(II) (Figure 5a).

While intermediate applied potentials (−0.61 and −1.01 V *vs.* SCE) do not change the structure of the catalyst, application of −1.31 *vs.* SCE results in gradual modification of the catalyst structure. At −1.31 V *vs.* SCE, new peaks can be observed in the *in situ* EXAFS (Figure 5b). Two new peaks are attributed to the formation of a small percentage of Fe metal centers, possibly in the form of Fe nanoparticles with the Fe−Fe distances close to metallic iron at ∼2.5 and ∼3.9 Å. An additional strong peak around ∼3.2 Å can be assigned to Fe(II) mono-μ-oxo bridges, the formation of which likely precedes the conversion of the single Fe centers into the Fe metallic phase. Catalyst transformation is particularly prominent in the absence of NO_3^- substrate. EXAFS fits confirm the above tentative assignment of the new peaks (Table S3 and Figure S32). EXAFS fits are in agreement with XANES analysis, which indicates ∼1.5% content of Fe metal nanoparticles.

The presence of NO_3^- substrate (20 mM $NaNO_3$) does not change the reductive progression in the XANES spectra. *In situ* Fe XANES is similar with and without the substrate,

https://doi.org/10.1021/jacs.2c03487
J. Am. Chem. Soc. 2022, 144, 17824−17831

corresponding to the Fe(II) state after ∼2 h at −1.31 V *vs.* SCE. The presence of substrate slows the rate of catalyst conversion to new forms at −1.31 V *vs.* SCE. Other than the different content of peaks assigned to Fe−Fe and Fe−O−Fe interactions of the modified electrode, the main effect of the substrate is the shift of the first EXAFS peak (Fe−N interaction) to a shorter distance (Figure 6). This is clearly visible in the Fourier transform spectra and detected in the EXAFS fits (Table S4 and Figure S33). It is impossible to fit the first peak satisfactorily unless the short Fe−N distance is included.

The short Fe−N distance (∼1.65 Å) is consistent with that observed in $\{Fe(NO)\}^6$ complexes, suggesting that electrocatalytic nitrate reduction involves the formation of an iron nitrosyl intermediate.[54−56] This hypothesis is supported by previous work, which has demonstrated that iron nitrosyl complexes (e.g., $[Fe(NO)(TPPS)]^{3-}$) can be prepared *via* the proton-coupled reduction of aqueous nitrite.[57] Other intermediates with short Fe−N bonds, including Fe≡N and Fe═N−H, are less likely. For instance, the Fe−N distance determined by EXAFS (∼1.65 Å) is longer than observed molecular iron nitride complexes, where Fe≡N < 1.6 Å. Although no structurally characterized Fe═N−H complexes are known, similar Fe−N bond distances have been observed for some Fe(IV) and Fe(V) alkyl and tosylimido complexes; however, these high oxidation states are unlikely to be stable under the reducing electrocatalysis conditions. In addition, while certain low valent alkyl and aryl imido complexes also have a similar Fe−N bond length, the iron center has a low coordination number (≤4) in these complexes (see Tables S7 and S8 for details).

Further evidence for the formation of a nitrosyl ligand comes from XPS. Here, a new peak at 402.8 eV is observed in the high-resolution N 1s spectrum recorded immediately after CPE at −1.31 V *vs.* SCE in the presence of 20 mM $NaNO_3$ (Figure S38). This binding energy is similar to that reported for other iron nitrosyl complexes.[58,59] In addition, the high-resolution O 1s spectrum shows a peak at 530.8 eV, which is also consistent with that observed for iron nitrosyl complexes (Figure S39). The high-resolution Fe 2p spectrum indicates the presence of both Fe(II) and Fe(III), with no evidence for metallic iron (Figure S41).

These conclusions are supported by the results of DFT calculations for the model system, where the computed bond metrics for the iron nitrosyl $\{FeNO\}^6$ are most consistent with the experimental data (see Tables S11 and S12). Both five-coordinate and six-coordinate complexes were considered as the candidates, and a low-spin six-coordinate complex with the OH^- trans to the nitrosyl showed the best match between the experimentally determined (1.65 Å) and the calculated (1.64 Å) FeN bond length. The complex corresponds to a low-spin Fe(II) species, with two of the doubly occupied t_{2g} orbitals of Fe showing significant back-bonding interactions with the π^* orbitals of the nitrosyl ligand (see Figure S54).

Interestingly, *ex situ* XAS data from a "spent" GCC-FeDIM electrode (dried after 3 h at −1.31 V *vs.* SCE applied potential in 0.5 M Na_2SO_4 and 20 mM $NaNO_3$) shows only the Fe(III) oxidation state (Figure S34). Thus, the catalytically active Fe(II) state can only be observed *in situ*, and all Fe centers are reoxidized to Fe(III) upon termination of electrolysis. A small modification in the pre-edge intensity of the "spent" GCC-FeDIM electrode can be accounted for by adding ∼1.5% of the Fe metal spectrum to the initial pristine GCC-FeDIM electrode spectrum (Figure S34). Similar modification of the pre-edge is visible in the *in situ* data as well. This, in addition, confirms the presence of Fe metal as a result of the electrochemical transformations; however, the content of modified Fe centers is very small. Formation of metallic Fe on the Grafoil surface implies that the deactivation pathway of the GCC-FeDIM catalyst includes Fe(II) demetallation and possible further binding to available Fe centers with the formation of Fe−O−Fe species, which can be further reduced to metallic iron.

CONCLUSIONS

Spectroscopic characterization of the readily assembled graphite-conjugated macrocycle catalyst, GCC-FeDIM, reveals that the surface of the graphite electrode is decorated with high spin (S = 5/2) Fe(III) sites in an FeN_4Cl_2 coordination environment. The chloride ligands are hydrolyzed in aqueous solution, with proton-coupled electron transfer affording Fe(II)-OH_2 sites on reduction, as supported by the results of DFT calculations. Electrocatalytic experiments show that GCC-FeDIM is among the fastest known electrocatalysts for the reduction of aqueous NO_3^-, producing ammonium with high Faradaic efficiency. More importantly, the well-defined nature of the iron centers in GCC-FeDIM allows for the spectroscopic characterization of a catalytic intermediate, which is proposed to be an iron nitrosyl from experimental and computational mechanistic studies. To the best of our knowledge, this is the first observation of an intermediate in the reduction of nitrate by a heterogeneous electrocatalyst.

Based on the foregoing results, we expect that the highly tunable molecular environment exemplified by GCC-FeDIM will allow structure/function relationships in heterogeneous nitrate reduction electrocatalysis to be established. Moreover, we anticipate that the system will provide a platform for similar insight into the mechanisms of other heterogeneous electrocatalysts.

ASSOCIATED CONTENT

Supporting Information

The Supporting Information is available free of charge at https://pubs.acs.org/doi/10.1021/jacs.2c03487.

Additional experimental details, materials, and methods (PDF)

Structures of the complexes mentioned in this work (XYZ)

AUTHOR INFORMATION

Corresponding Authors

Elena Jakubikova − *Department of Chemistry, North Carolina State University, Raleigh, North Carolina 27695, United States;* orcid.org/0000-0001-7124-8300; Email: ejakubi@ncsu.edu

Yulia N. Pushkar − *Department of Physics, Purdue University, West Lafayette, Indiana 47907, United States;* orcid.org/0000-0001-7949-6472; Email: ypushkar@purdue.edu

Jeremy M. Smith − *Department of Chemistry, Indiana University, Bloomington, Indiana 47401, United States;* orcid.org/0000-0002-3206-4725; Email: smith962@indiana.edu

Authors

Moumita Ghosh − *Department of Chemistry, Indiana University, Bloomington, Indiana 47401, United States*

Sarah E. Braley − *Department of Chemistry, Indiana University, Bloomington, Indiana 47401, United States*

Roman Ezhov − *Department of Physics, Purdue University, West Lafayette, Indiana 47907, United States;* orcid.org/0000-0001-6806-4033

Harrison Worster − *Department of Chemistry, North Carolina State University, Raleigh, North Carolina 27695, United States*

Juan A. Valdez-Moreira − *Department of Chemistry, Indiana University, Bloomington, Indiana 47401, United States*

Yaroslav Losovyj − *Department of Chemistry, Indiana University, Bloomington, Indiana 47401, United States*

Complete contact information is available at: https://pubs.acs.org/10.1021/jacs.2c03487

Notes

The authors declare no competing financial interest.

■ ACKNOWLEDGMENTS

We gratefully acknowledge funding from the NSF (CHE-2102440 to YNP, CHE-2102442 to JMS, CHE-2102497 to EJ). The use of the Advanced Photon Source, an Office of Science User Facility operated by the US Department of Energy (DOE) Office of Science by Argonne National Laboratory, was supported by the US DOE under contract DE-AC02-06CH11357. The PNC/XSD (Sector 20) facilities at the Advanced Photon Source and research at these facilities were supported by the US Department of Energy, Basic Energy Science and the Canadian Light Source. Access to EPR was provided by the Amy Instrumentation Facility, Department of Chemistry, under the supervision of Dr. Michael Everly. We acknowledge Gabriel Bury for his assistance in recording EPR spectra. M.G. and J.M.S. thank Courtney Mobillin and Shelby Rader for assistance with the ion chromatography and ICP-MS, respectively. We thank Nayana Christudas Beena for assistance with TCD-GC.

■ REFERENCES

(1) Erisman, J. W.; Sutton, M. A.; Galloway, J.; Klimont, Z.; Winiwarter, W. How a century of ammonia synthesis changed the world. *Nat. Geosci.* **2008**, *1*, 636.

(2) Smil, V. Nitrogen Cycle and World Food Production. *World Agric.* **2011**, *2*, 9.

(3) Godfray, H. C. J.; Beddington, J. R.; Crute, I. R.; Haddad, L.; Lawrence, D.; Muir, J. F.; Pretty, J.; Robinson, S.; Thomas, S. M.; Toulmin, C. Food Security: The Challenge of Feeding 9 Billion People. *Science* **2010**, *327*, 812.

(4) Smil, V. *Enriching the Earth: Fritz Haber, Carl Bosch and the Transformation of World Food Production*; MIT Press: Cambridge, 2001.

(5) Matassa, S.; Batstone, D. J.; Hülsen, T.; Schnoor, J.; Verstraete, W. Can Direct Conversion of Used Nitrogen to New Feed and Protein Help Feed the World? *Environ. Sci. Technol.* **2015**, *49*, 5247.

(6) Galloway, J. N.; Aber, J. D.; Erisman, J. W.; Seitzinger, S. P.; Howarth, R. W.; Cowling, E. B.; Cosby, B. J. The Nitrogen Cascade. *BioScience* **2003**, *53*, 341.

(7) Fowler, D.; Coyle, M.; Skiba, U.; Sutton, M. A.; Cape, J. N.; Reis, S.; Sheppard, L. J.; Jenkins, A.; Grizzetti, B.; Galloway, J. N.; Vitousek, P.; Leach, A.; Bouwman, A. F.; Butterbach-Bahl, K.; Dentener, F.; Stevenson, D.; Amann, M.; Voss, M. The global nitrogen cycle in the twenty-first century. *Philos. Trans. R. Soc., B* **2013**, *368*, 20130164.

(8) Sebilo, M.; Mayer, B.; Nicolardot, B.; Pinay, G.; Mariotti, A. Long-term fate of nitrate fertilizer in agricultural soils. *Proc. Natl. Acad. Sci. U. S. A.* **2013**, *110*, 18185.

(9) *Wastewater: The Untapped Resource*; United Nations World Water: 22 March, 2017.

(10) Taniguchi, L.; Nakashima, N.; Yasukouchi, K. Reduction of nitrate to give hydroxylamine at a mercury electrode using cobalt(III) and nickel(II)−cyclams as catalysts. *J. Chem. Soc., Chem. Commun.* **1986**, 1814.

(11) Rosca, V.; Duca, M.; de Groot, M. T.; Koper, M. T. M. Nitrogen Cycle Electrocatalysis. *Chem. Rev.* **2009**, *109*, 2209.

(12) Xu, S.; Ashley, D. C.; Kwon, H.-Y.; Ware, G. R.; Chen, C.-H.; Losovyj, Y.; Gao, X.; Jakubikova, E.; Smith, J. M. A flexible, redox-active macrocycle enables the electrocatalytic reduction of nitrate to ammonia by a cobalt complex. *Chem. Sci.* **2018**, *9*, 4950.

(13) Taniguchi, I.; Nakashima, N.; Matsushita, K.; Yasukouchi, K. Electrocatalytic reduction of nitrate and nitrite to hydroxylamine and ammonia using metal cyclams. *J. Electroanal. Chem. Interfac. Electrochem.* **1987**, *224*, 199.

(14) Chebotareva, N.; Nyokong, T. Metallophthalocyanine catalysed electroreduction of nitrate and nitrite ions in alkaline media. *J. Appl. Electrochem.* **1997**, *27*, 975.

(15) Yoshioka, T.; Iwase, K.; Nakanishi, S.; Hashimoto, K.; Kamiya, K. Electrocatalytic Reduction of Nitrate to Nitrous Oxide by a Copper-Modified Covalent Triazine Framework. *J. Phys. Chem. C* **2016**, *120*, 15729.

(16) Shen, J.; Birdja, Y. Y.; Koper, M. T. M. Electrocatalytic Nitrate Reduction by a Cobalt Protoporphyrin Immobilized on a Pyrolytic Graphite Electrode. *Langmuir* **2015**, *31*, 8495.

(17) Zhang, X.; Wang, Y.; Liu, C.; Yu, Y.; Lu, S.; Zhang, B. Recent advances in non-noble metal electrocatalysts for nitrate reduction. *Chem. Eng. J.* **2021**, *403*, 126269.

(18) Dima, G. E.; de Vooys, A. C. A.; Koper, M. T. M. Electrocatalytic reduction of nitrate at low concentration on coinage and transition-metal electrodes in acid solutions. *J. Electroanal. Chem.* **2003**, *554-555*, 15.

(19) Liu, J.-X.; Richards, D.; Singh, N.; Goldsmith, B. R. Activity and Selectivity Trends in Electrocatalytic Nitrate Reduction on Transition Metals. *ACS Catal.* **2019**, *9*, 7052.

(20) Ma, Y.; Han, X.; Xu, S.; Wang, Z.; Li, W.; da Silva, I.; Chansai, S.; Lee, D.; Zou, Y.; Nikiel, M.; Manuel, P.; Sheveleva, A. M.; Tuna, F.; McInnes, E. J. L.; Cheng, Y.; Rudić, S.; Ramirez-Cuesta, A. J.; Haigh, S. J.; Hardacre, C.; Schröder, M.; Yang, S. Atomically Dispersed Copper Sites in a Metal−Organic Framework for Reduction of Nitrogen Dioxide. *J. Am. Chem. Soc.* **2021**, *143*, 10977.

(21) Liu, H.; Park, J.; Chen, Y.; Qiu, Y.; Cheng, Y.; Srivastava, K.; Gu, S.; Shanks, B. H.; Roling, L. T.; Li, W. Electrocatalytic Nitrate Reduction on Oxide-Derived Silver with Tunable Selectivity to Nitrite and Ammonia. *ACS Catal.* **2021**, 8431.

(22) Wu, Z.-Y.; Karamad, M.; Yong, X.; Huang, Q.; Cullen, D. A.; Zhu, P.; Xia, C.; Xiao, Q.; Shakouri, M.; Chen, F.-Y.; Kim, J. Y.; Xia, Y.; Heck, K.; Hu, Y.; Wong, M. S.; Li, Q.; Gates, I.; Siahrostami, S.; Wang, H. Electrochemical ammonia synthesis *via* nitrate reduction on Fe single atom catalyst. *Nat. Commun.* **2021**, *12*, 2870.

(23) Xu, S.; Kwon, H.-Y.; Ashley, D. C.; Chen, C.-H.; Jakubikova, E.; Smith, J. M. Intramolecular Hydrogen Bonding Facilitates Electrocatalytic Reduction of Nitrite in Aqueous Solutions. *Inorg. Chem.* **2019**, *58*, 9443.

(24) Jackson, M. N.; Jung, O.; Lamotte, H. C.; Surendranath, Y. Donor-Dependent Promotion of Interfacial Proton-Coupled Electron Transfer in Aqueous Electrocatalysis. *ACS Catal.* **2019**, *9*, 3737.

(25) Jackson, M. N.; Oh, S.; Kaminsky, C. J.; Chu, S. B.; Zhang, G.; Miller, J. T.; Surendranath, Y. Strong Electronic Coupling of Molecular Sites to Graphitic Electrodes *via* Pyrazine Conjugation. *J. Am. Chem. Soc.* **2018**, *140*, 1004.

(26) Blakemore, J. D.; Gupta, A.; Warren, J. J.; Brunschwig, B. S.; Gray, H. B. Noncovalent Immobilization of Electrocatalysts on Carbon Electrodes for Fuel Production. *J. Am. Chem. Soc.* **2013**, *135*, 18288.

(27) Mann, J. A.; Rodríguez-López, J.; Abruña, H. D.; Dichtel, W. R. Multivalent Binding Motifs for the Noncovalent Functionalization of Graphene. *J. Am. Chem. Soc.* **2011**, *133*, 17614.
(28) Delamar, M.; Hitmi, R.; Pinson, J.; Saveant, J. M. Covalent modification of carbon surfaces by grafting of functionalized aryl radicals produced from electrochemical reduction of diazonium salts. *J. Am. Chem. Soc.* **1992**, *114*, 5883.
(29) Sheridan, M. V.; Lam, K.; Geiger, W. E. An Anodic Method for Covalent Attachment of Molecules to Electrodes through an Ethynyl Linkage. *J. Am. Chem. Soc.* **2013**, *135*, 2939.
(30) Kaminsky, C. J.; Wright, J.; Surendranath, Y. Graphite-Conjugation Enhances Porphyrin Electrocatalysis. *ACS Catal.* **2019**, *9*, 3667.
(31) Fukushima, T.; Drisdell, W.; Yano, J.; Surendranath, Y. Graphite-Conjugated Pyrazines as Molecularly Tunable Heterogeneous Electrocatalysts. *J. Am. Chem. Soc.* **2015**, *137*, 10926.
(32) Braley, S. E.; Xie, J.; Losovyj, Y.; Smith, J. M. Graphite Conjugation of a Macrocyclic Cobalt Complex Enhances Nitrite Electroreduction to Ammonia. *J. Am. Chem. Soc.* **2021**, *143*, 7203.
(33) Yamashita, T.; Hayes, P. Analysis of XPS spectra of Fe^{2+} and Fe^{3+} ions in oxide materials. *Appl. Surf. Sci.* **2008**, *254*, 2441.
(34) Wagner, C. D. *The NIST X-ray Photoelectron Spectroscopy (XPS) Database*; NIST: Washington, D.C, 1991.
(35) Zhang, H. L.; Hirschmann, M. M.; Cottrell, E.; Newville, M.; Lanzirotti, A. Structural environment of iron and accurate determination of $Fe^{3+}/\Sigma Fe$ ratios in andesitic glasses by XANES and Mössbauer spectroscopy. *Chem. Geol.* **2016**, *428*, 48.
(36) Meyer, K.; Bill, E.; Mienert, B.; Weyhermüller, T.; Wieghardt, K. Photolysis of *cis*- and *trans*-$[Fe^{III}(cyclam)(N_3)^2]^+$ Complexes: Spectroscopic Characterization of a Nitridoiron(V) Species. *J. Am. Chem. Soc.* **1999**, *121*, 4859.
(37) Guilard, R.; Siri, O.; Tabard, A.; Broeker, G.; Richard, P.; Nurco, D. J.; Smith, K. M. One-pot synthesis, physicochemical characterization and crystal structures of *cis*- and *trans*-(1,4,8,11-tetraazacyclotetradecane)-dichloroiron(III) complexes. *J. Chem. Soc., Dalton Trans.* **1997**, 3459.
(38) Clendening, R. A.; Zeller, M.; Ren, T. Crystal structures of two (5,5,7,12,12,14-hexamethyl-1,4,8,11-tetraazacyclotetradecane)iron-(III) complexes. *Acta Crystallogr., Sect. C: Struct. Chem.* **2019**, *75*, 1509.
(39) Chun, H.; Bill, E.; Bothe, E.; Weyhermüller, T.; Wieghardt, K. Octahedral (*cis*-Cyclam)iron(III) Complexes with O,N-Coordinated o-Iminosemiquinonate(1−) π Radicals and o-Imidophenolate(2−) Anions. *Inorg. Chem.* **2002**, *41*, 5091.
(40) Safo, M. K.; Gupta, G. P.; Watson, C. T.; Simonis, U.; Walker, F. A.; Scheidt, W. R. Models of the cytochromes b. Low-spin bis-ligated (porphinato)iron(III) complexes with unusual molecular structures and NMR, EPR, and Moessbauer spectra. *J. Am. Chem. Soc.* **1992**, *114*, 7066.
(41) Rountree, E. S.; McCarthy, B. D.; Eisenhart, T. T.; Dempsey, J. L. Evaluation of Homogeneous Electrocatalysts by Cyclic Voltammetry. *Inorg. Chem.* **2014**, *53*, 9983.
(42) Weatherburn, M. W. Phenol-hypochlorite reaction for determination of ammonia. *Anal. Chem.* **1967**, *39*, 971.
(43) Li, P.; Jin, Z.; Fang, Z.; Yu, G. A single-site iron catalyst with preoccupied active centers that achieves selective ammonia electrosynthesis from nitrate. *Energy Environ. Sci.* **2021**, *14*, 3522.
(44) Liu, Y.; Wang, J. Reduction of nitrate by zero valent iron (ZVI)-based materials: A review. *Sci. Total Environ.* **2019**, *671*, 388.
(45) Partovi, S.; Xiong, Z.; Kulesa, K. M.; Smith, J. M. Electrocatalytic Reduction of Nitrogen Oxyanions with a Redox-Active Cobalt Macrocycle Complex. *Inorg. Chem.* **2022**, *61*, 9034.
(46) Chen, S.-S.; Hsu, H.-D.; Li, C.-W. A new method to produce nanoscale iron for nitrate removal. *J. Nanopart. Res.* **2004**, *6*, 639.
(47) Shin, H.; Jung, S.; Bae, S.; Lee, W.; Kim, H. Nitrite Reduction Mechanism on a Pd Surface. *Environ. Sci. Technol.* **2014**, *48*, 12768.
(48) Chun, H.-J.; Apaja, V.; Clayborne, A.; Honkala, K.; Greeley, J. Atomistic Insights into Nitrogen-Cycle Electrochemistry: A Combined DFT and Kinetic Monte Carlo Analysis of NO Electrochemical Reduction on Pt(100). *ACS Catal.* **2017**, *7*, 3869.
(49) Ford, C. L.; Park, Y. J.; Matson, E. M.; Gordon, Z.; Fout, A. R. A bioinspired iron catalyst for nitrate and perchlorate reduction. *Science* **2016**, *354*, 741.
(50) Suslick, K. S.; Watson, R. A. Photochemical reduction of nitrate and nitrite by manganese and iron porphyrins. *Inorg. Chem.* **1991**, *30*, 912.
(51) Tsai, F.-T.; Lee, Y.-C.; Chiang, M.-H.; Liaw, W.-F. Nitrate-to-Nitrite-to-Nitric Oxide Conversion Modulated by Nitrate-Containing $\{Fe(NO)_2\}^9$ Dinitrosyl Iron Complex (DNIC). *Inorg. Chem.* **2013**, *52*, 464.
(52) Delgado, M.; Gilbertson, J. D. Ligand-based reduction of nitrate to nitric oxide utilizing a proton-responsive secondary coordination sphere. *Chem. Commun.* **2017**, *53*, 11249.
(53) Beagan, D. M.; Carta, V.; Caulton, K. G. A reagent for heteroatom borylation, including iron mediated reductive deoxygenation of nitrate yielding a dinitrosyl complex. *Dalton Trans.* **2020**, *49*, 1681.
(54) Wyllie, G. R. A.; Scheidt, W. R. Solid-State Structures of Metalloporphyrin NO_x Compounds. *Chem. Rev.* **2002**, *102*, 1067.
(55) Kupper, C.; Rees, J. A.; Dechert, S.; DeBeer, S.; Meyer, F. Complete Series of $\{FeNO\}^8$, $\{FeNO\}^7$, and $\{FeNO\}^6$ Complexes Stabilized by a Tetracarbene Macrocycle. *J. Am. Chem. Soc.* **2016**, *138*, 7888.
(56) Holanda, A. K. M.; da Silva, F. O. N.; Carvalho, I. M. M.; Batista, A. A.; Ellena, J.; Castellano, E. E.; Moreira, Í. S.; Lopes, L. G. F. Crystal structure, electrochemical and photochemical studies of the *trans*-$[Fe(cyclam)(NO)Cl]Cl_2$ complex (cyclam=1,4,8,11-tetraazacyclotetradecane). *Polyhedron* **2007**, *26*, 4653.
(57) Barley, M. H.; Meyer, T. J. Electrocatalytic reduction of nitrite to ammonia based on a water-soluble iron porphyrin. *J. Am. Chem. Soc.* **1986**, *108*, 5876.
(58) Cano, A.; Lartundo-Rojas, L.; Shchukarev, A.; Reguera, E. Contribution to the coordination chemistry of transition metal nitroprussides: a cryo-XPS study. *New J. Chem.* **2019**, *43*, 4835.
(59) Isvoranu, C.; Wang, B.; Ataman, E.; Knudsen, J.; Schulte, K.; Andersen, J. N.; Bocquet, M.-L.; Schnadt, J. Comparison of the Carbonyl and Nitrosyl Complexes Formed by Adsorption of CO and NO on Monolayers of Iron Phthalocyanine on Au(111). *J. Phys. Chem. C* **2011**, *115*, 24718.

https://doi.org/10.1021/jacs.2c03487
J. Am. Chem. Soc. 2022, 144, 17824−17831